MADRID
inter.noise 2019
June 16 - 19
NOISE CONTROL FOR A BETTER ENVIRONMENT

Vibro-acoustic coupling analysis of the orthotropic annular sector double-plate coupled with an acoustic cavity

Wang, Yuanda[1]
College of Mechanical and Electrical Engineering, Harbin Engineering University
No.145 Nantong Street, Nangang District, Harbin, Heilongjiang Prov., P.R. China

Shi, Dongyan[2]
College of Mechanical and Electrical Engineering, Harbin Engineering University
No.145 Nantong Street, Nangang District, Harbin, Heilongjiang Prov., P.R. China

Zhang, Hong[3]
National Key Laboratory of Science and Technology on Helicopter Transmission, Nanjing University of Aeronautics and Astronautics
No.29 Yudao Street, Qinhuai District, Nanjing, Jiangsu Prov., P.R. China

Zha, Shuai[4]
College of Mechanical and Electrical Engineering, Harbin Engineering University
No.145 Nantong Street, Nangang District, Harbin, Heilongjiang Prov., P.R. China

ABSTRACT

In this investigation, a structural-acoustic coupling model is established, which is composed of the thin orthotropic annular sector parallel double-plate with various elastic boundary conditions and an acoustic cavity with various impedance walls. Under the current framework, the admissible displacement and sound pressure of the coupling system are generally expressed as superposition of simple periodic functions on the basis of the modified Fourier series method. The setting of the elastic boundary conditions is realized by artificial virtual spring technology. The vibro-acoustic characteristics can be obtained by Rayleigh-Ritz technique. Unlike most of the existing studies, the presented method can be readily applied to a wide spectrum of the vibro-acoustic problems with no need of modifying the basic functions or adapting solution procedures, such as different boundary conditions, varying materials and geometric parameters. The fast convergence of the present method has been given by selecting smaller truncation values. In addition, the accuracy of the present method has been proved by being compared with the finite element method (FEM). Numerous new results are also presented which can be the benchmark for the future research.

[1] wangyuanda@hrbeu.edu.cn
[2] shidongyan@ hrbeu.edu.cn
[3] zhanghong@ hrbeu.edu.cn
[4] zhashuai@ hrbeu.edu.cn

Keywords: Vibro-acoustic coupling analysis, elastic boundary conditions, various impedance walls, modified Fourier series method, Rayleigh-Ritz technique.
I-INCE Classification of Subject Number: 42

1. INTRODUCTION

In the context of the extensive use of orthotropic material in engineering applications, many models could be abstracted into a fluid-structure coupling system composed of an acoustic cavity and the orthotropic annular sector parallel double-plate. Therefore, it is of great practical significance to establish an effective analytical model to explore the coupled mechanism and the vibro-acoustic characteristics, which can satisfy higher requirements of vibration and low noise control.

There have been some literatures for the rotational structural-acoustic coupling systems including both the structure domain and the sound field. Li *et al*. [1] proposed a method of Radiation Efficiency Analysis of Structural Modes to study the sound-vibration coupled characteristics of the cylindrical shell coupled with internal floor partition. Henry *et al*. [2, 3] established a model composed of a typical aircraft plate coupled with a rigid-wall cylinder with attached piezoelectric actuators in service conditions to realize the active control of sound transmission. Gardonio *et al*. [4] investigated the plane wave transmission characteristics of the circular cylindrical sandwich shell in the aerospace industry for satellite launch vehicles based on a modal interaction analysis (MIA). Lee *et al*. [5] examined the insertion loss of a cavity-backed semi-cylindrical enclosure panel, and the theoretical results were validated by the experimental results. According to a circularly metamaterial model, Yao *et al*. [6] analyzed the sound radiation properties based on the numerical simulations for structured metamaterials. It was found that it is an efficient method to reduce the sound vibration over the negative-mass frequencies with increasing the thickness of the metamaterial barrier. Rocha *et al*. [7] established a structural-acoustic coupling system composed of aircraft cabin section and the fuselage structure to predict turbulent boundary-layer-induced noise in the interior of aircraft cylindrical cabins. Pan *et al*. [8] modeled and analyzed the noise radiation of a cylindrical enclosure on the excitation of the internal acoustic which placed inside the water. From these researches, we can find that there are few studies on the interaction and coupling mechanism of the structure-acoustic coupled system. In addition, the elastic plates in the above studies are mostly single plates rather than double plates, and the filling materials are mostly isotropic rather than orthotropic.

In view of the limitations of existing research, this paper establishes an orthotropic annular sector double-plate cavity coupling system to study the vibro-acoustic coupling characteristics. The correctness of the established analytical model has been validated by being compared with the results achieved by FEM. On this basis, some new results and conclusions are given.

2. THEORETICAL FORMULATIONS

2.1 Description of The Structural-Acoustic Coupling System

As shown in Figure 1, the coordinate system and geometry model of the structural-acoustic coupling system with the elastic boundary conditions are given here which can effectively study the vibro-acoustic coupling characteristics. This coupling system is composed of the thin orthotropic annular sector parallel double-plate with various elastic boundary conditions and an acoustic cavity with various impedance walls. First of all, an integral cylindrical coordinate system (O- $r\theta z$) and a local coordinate system (O′ - $s\theta z$)

for this coupled model are established. s represents the difference between the out radius R_1 and the inner radius R_0. In addition, θ and z are represented as the angle and height directions of studied model. For the annular segment plates and acoustic cavity, the same dimensions are outer radius, inner radius and sector angle dimensions (ϕ), respectively. In this model, the thickness of upper plate is marked as h_{p1}, and the thickness of lower plate is marked as h_{p2}, separately. In addition, the thickness of the cavity is donated as h_c. The boundary conditions are simulated by artificial spring technology. As shown in Figure 1, the boundary spring is composed of the linear spring (k^w) and the rotating spring (K^w) evenly distributed on the four edges of the orthotropic plate. In order to further study the vibro-acoustic characteristics of the coupling system, the point sound source Q placed inside the cavity can be added to study the coupling response.

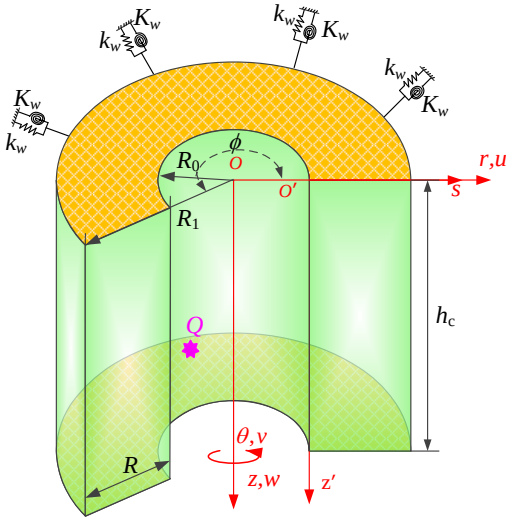

***Figure 1**:The coordinate system and geometry model of the annular sector parallel double-plate-cavity coupling system with various elastic boundary conditions*

2.2 Admissible Functions of Displacements and Sound Pressure

In this paper, a modified Fourier series method is applied to represent the displacement functions of the orthotropic thin plate and the sound pressure functions of the cavity. The expression is a form of superposition functions, consisting of the product of cosine functions and supplementary polynomials. The admissible vector functions of double-plate-cavity are written as:

$$w_g(s,\theta)=\left(\mathbf{W}^{\Omega}(x,y)+\sum_{l=1}^{2}\mathbf{W}_l^{\mathrm{B}}(x,y)\right)\mathbf{A}_{mn}^{g} \tag{1}$$

$$p(s,\theta,z)=\left(\mathbf{P}^{\Omega}(s,\theta,z)+\sum_{i=1}^{6}\mathbf{P}_i^{\mathrm{S}}(s,\theta,z)\right)\mathbf{C}_{m_1n_1l_1} \tag{2}$$

where the displacement of the plate is marked as w_g (g=1,2). It should be pointed out that the g=1is for the upper plate and g=2 is for the lower plate. The internal displacement vector and the supplementary polynomials are expressed as $\mathbf{W}^{\Omega}$ and $\mathbf{W}_l^{\mathrm{B}}$ (l =1, 2). Besides, the sound pressure expression and the supplementary polynomials of the cavity are represented as $\mathbf{P}^{\Omega}$ and $\mathbf{P}_i^{\mathrm{S}}$ (i =1-6). The unknown Fourier vectors are $\mathbf{A}_{mn}^{g}$ and $\mathbf{C}_{m_1n_1l_1}$, which can be written as:

$$\mathbf{W}^{\Omega}=\begin{Bmatrix}\cos\lambda_0^a x\cos\lambda_0^b y,\cdots,\cos\lambda_0^a x\cos\lambda_n^b y,\cdots,\\ \cos\lambda_0^a x\cos\lambda_N^b y,\cdots,\cos\lambda_M^a x\cos\lambda_N^b y\end{Bmatrix} \tag{3a}$$

$$\mathbf{W}_1^{\mathrm{B}}=\begin{Bmatrix}\sin(\lambda_{-2}^{a}x)\cos(\lambda_{0}^{b}y),\cdots,\sin(\lambda_{-2}^{a}x)\cos(\lambda_{n}^{b}y),\cdots,\\ \sin(\lambda_{-2}^{a}x)\cos(\lambda_{N}^{b}y),\cdots,\sin(\lambda_{-1}^{a}x)\cos(\lambda_{N}^{b}y)\end{Bmatrix} \tag{3b}$$

$$\mathbf{P}^{\Omega}(x,y,z)=\begin{Bmatrix}\cos\lambda_{0}^{a}x\cos\lambda_{0}^{b}y\cos\lambda_{0}^{h_c}z,\cdots,\cos\lambda_{0}^{a}x\cos\lambda_{0}^{b}y\cos\lambda_{L_1}^{h_c}z,\cdots,\\ \cos\lambda_{0}^{a}x\cos\lambda_{N_1}^{b}y\cos\lambda_{L_1}^{h_c}z,\cdots,\cos\lambda_{M_1}^{a}x\cos\lambda_{N_1}^{b}y\cos\lambda_{L_1}^{h_c}z\end{Bmatrix} \tag{4a}$$

$$\mathbf{P}^{\mathrm{S}_1}(x,y,z)=\begin{Bmatrix}\sin\lambda_{-2}^{a}x\cos\lambda_{0}^{b}y\cos\lambda_{0}^{h_c}z,\cdots,\sin\lambda_{-2}^{a}x\cos\lambda_{0}^{b}y\cos\lambda_{L_1}^{h_c}z,\cdots,\\ \sin\lambda_{-2}^{a}x\cos\lambda_{N_1}^{b}y\cos\lambda_{L_1}^{h_c}z,\cdots,\sin\lambda_{-1}^{a}x\cos\lambda_{N_1}^{b}y\cos\lambda_{L_1}^{h_c}z\end{Bmatrix} \tag{4b}$$

$$\mathbf{P}^{\mathrm{S}_2}(x,y,z)=\begin{Bmatrix}\cos\lambda_{0}^{a}x\sin\lambda_{-2}^{b}y\cos\lambda_{0}^{h_c}z,\cdots,\cos\lambda_{0}^{a}x\sin\lambda_{-2}^{b}y\cos\lambda_{L_1}^{h_c}z,\cdots,\\ \cos\lambda_{0}^{a}x\sin\lambda_{-2}^{b}y\cos\lambda_{L_1}^{h_c}z,\cdots,\cos\lambda_{M_1}^{a}x\sin\lambda_{-1}^{b}y\cos\lambda_{L_1}^{h_c}z\end{Bmatrix} \tag{4c}$$

$$\mathbf{P}^{\mathrm{S}_3}(x,y,z)=\begin{Bmatrix}\cos\lambda_{0}^{a}x\cos\lambda_{0}^{b}y\sin\lambda_{-2}^{h_c}z,\cos\lambda_{0}^{a}x\cos\lambda_{0}^{b}y\sin\lambda_{-1}^{h_c}z,\cdots,\\ \cos\lambda_{0}^{a}x\cos\lambda_{N_1}^{b}y\sin\lambda_{-2}^{h_c}z,\cdots,\cos\lambda_{M_1}^{a}x\cos\lambda_{N_1}^{b}y\sin\lambda_{-1}^{h_c}z\end{Bmatrix} \tag{4d}$$

$$\mathbf{P}^{\mathrm{S}_4}(x,y,z)=\begin{Bmatrix}\sin\lambda_{-2}^{a}x\sin\lambda_{-2}^{b}y\cos\lambda_{0}^{h_c}z,\cdots,\sin\lambda_{-2}^{a}x\sin\lambda_{-2}^{b}y\cos\lambda_{L_1}^{h_c}z,\cdots,\\ \sin\lambda_{-2}^{a}x\sin\lambda_{-1}^{b}y\cos\lambda_{L_1}^{h_c}z,\cdots,\sin\lambda_{-1}^{a}x\sin\lambda_{-1}^{b}y\cos\lambda_{L_1}^{h_c}z\end{Bmatrix} \tag{4e}$$

$$\mathbf{P}^{\mathrm{S}_5}(x,y,z)=\begin{Bmatrix}\sin\lambda_{-2}^{a}x\cos\lambda_{0}^{b}y\sin\lambda_{-2}^{h_c}z,\sin\lambda_{-2}^{a}x\cos\lambda_{0}^{b}y\sin\lambda_{-1}^{h_c}z,\cdots,\\ \sin\lambda_{-2}^{a}x\cos\lambda_{N_1}^{b}y\sin\lambda_{-2}^{h_c}z,\cdots,\sin\lambda_{-1}^{a}x\cos\lambda_{N_1}^{b}y\sin\lambda_{-1}^{h_c}z\end{Bmatrix} \tag{4f}$$

$$\mathbf{P}^{\mathrm{S}_6}(x,y,z)=\begin{Bmatrix}\cos\lambda_{0}^{a}x\sin\lambda_{-2}^{b}y\sin\lambda_{-2}^{h_c}z,\cos\lambda_{0}^{a}x\sin\lambda_{-2}^{b}y\sin\lambda_{-1}^{h_c}z,\\ \cos\lambda_{0}^{a}x\sin\lambda_{-1}^{b}y\sin\lambda_{-2}^{h_c}z,\cdots,\cos\lambda_{M_1}^{a}x\sin\lambda_{-1}^{b}y\sin\lambda_{-1}^{h_c}z\end{Bmatrix} \tag{4g}$$

$$\mathbf{A}_{mn}^{g}=\begin{Bmatrix}A_{0,0}^{1},\cdots,A_{0,n}^{1},\cdots,A_{m,n}^{1},\cdots,A_{M,N}^{1},A_{-2,0}^{2},\cdots,A_{-2,n}^{2},\cdots,A_{-2,N}^{2},\cdots,A_{-1,N}^{2},\\ A_{0,-2}^{3},A_{0,-1}^{3},\cdots,A_{m,-2}^{3},\cdots,A_{M,-1}^{3}\end{Bmatrix}^{T} \tag{5}$$

$$\mathbf{C}_{m_1n_1l_1}=\begin{Bmatrix}C_{0,0,0}^{1},\cdots,C_{0,0,l_1}^{1},\cdots,C_{0,0,L_1}^{1},\cdots,C_{0,N_1,L_1}^{1},\cdots,C_{m_1,n_1,l_1}^{1},\cdots,C_{M_1,N_1,L_1}^{1},\\ C_{-2,0,0}^{2},\cdots,C_{-2,0,l_1}^{2},\cdots,C_{-2,0,L_1}^{2},\cdots,C_{-2,n_1,l_1}^{2},\cdots,C_{-1,n_1,l_1}^{2},\cdots,C_{-1,N_1,L_1}^{2},\\ C_{0,-2,0}^{3},\cdots,C_{0,-2,l_1}^{3},\cdots,C_{0,-2,L_1}^{3},\cdots,C_{m_1,-2,l_1}^{3},\cdots,C_{m_1,-1,l_1}^{3},\cdots,C_{M_1,-1,L_1}^{3},\\ C_{0,0,-2}^{4},C_{0,0,-1}^{4},\cdots,C_{0,N_1,-2}^{4},\cdots,C_{m_1,n_1,-2}^{4},\cdots,C_{m_1,n_1,-1}^{4},\cdots,C_{M_1,N_1,-1}^{4},\\ C_{-2,-2,0}^{5},\cdots,C_{-2,-2,l_1}^{5},\cdots,C_{-2,-2,L_1}^{5},\cdots,C_{-2,-1,l_1}^{5},\cdots,C_{-2,-1,L_1}^{5},\cdots,C_{-1,-1,L_1}^{5},\\ C_{-2,0,-2}^{6},C_{-2,0,-1}^{6},\cdots,C_{-2,n_1,-2}^{6},\cdots,C_{-2,N_1,-2}^{6},\cdots,C_{-1,n_1,L_1}^{6},\cdots,C_{-1,N_1,-1}^{6},\\ C_{0,-2,-2}^{7},C_{0,-2,-1}^{7},\cdots,C_{m_1,-2,-2}^{7},\cdots,C_{m_1,-1,-1}^{7},\cdots,C_{M_1,-2,-2}^{7},\cdots,C_{M_1,-1,-1}^{7}\end{Bmatrix}^{\mathrm{T}} \tag{6}$$

in which $\lambda_m=m\pi/a$, $\lambda_n=n\pi/b$, $\lambda_{m_1}^{a}=m_1\pi/a$, $\lambda_{n_1}^{b}=n_1\pi/b$, and $\lambda_{l_1}^{h_c}=l_1\pi/h_c$.

2.3 Energy Equation of the Structural-Acoustic Coupling System

In this section, the Lagrange energy equations of the coupling system are mainly described for the annular sector double-plate-cavity coupling system. First of all, the energy equations L_{plate}^{g} of the plate and the energy equations L_{cavity} of the cavity are given as follow:

$$L_{\mathrm{plate}}^{g}=T_{\mathrm{plate}}^{g}-U_{\mathrm{plate}}^{g}-V_{\mathrm{spring}}^{g}-W_{\mathrm{c\text{-}p}}^{g} \tag{7}$$

$$L_{\mathrm{cavity}}=T_{\mathrm{cavity}}-U_{\mathrm{cavity}}-W_{\mathrm{wall}}+W_{\mathrm{p\text{-}c}}^{1}+W_{\mathrm{p\text{-}c}}^{2}-W_{\mathrm{sound}} \tag{8}$$

in which T_{plate}^{g} and T_{cavity} are the total kinetic energy. U_{plate}^{g} and U_{cavity} are the total potential energy. V_{spring}^{g} is the spring potential energy stored at the boundaries. W_{wall} is the dissipated acoustic energy of the impedance walls. Besides, $W_{\text{c-p}}^{g}$ and $W_{\text{p-c}}^{g}$ are the interface coupling potential energy. In addition, W_{sound} is the work done by a point sound source.

The total kinetic energy equations T of the structural-acoustic coupling system are:

$$T_{\text{plate}}^{g}=\frac{\rho_{\text{pg}}h_{\text{pg}}\omega_{\text{pg}}^{2}}{2}\int_{R_0}^{R_1}\int_{0}^{\phi}\left\{\mathbf{A}_{mn}^{g}\left(\mathbf{W}^{\Omega}+\sum_{l=1}^{2}\mathbf{W}_{l}^{\text{B}}\right)\right\}^{2}rdrd\theta \tag{9}$$

$$T_{\text{cavity}}=\frac{1}{2\rho_{\text{c}}\omega_{\text{c}}^{2}}\int_{R_0}^{R_1}\int_{0}^{\phi}\int_{0}^{h_{\text{c}}}\left\{\begin{array}{l}\left(\dfrac{\partial\mathbf{P}^{\Omega}}{\partial x}+\sum_{i=1}^{6}\dfrac{\partial\mathbf{P}_{i}^{\text{S}}}{\partial x}\right)^{2}+\left(\dfrac{\partial\mathbf{P}^{\Omega}}{\partial y}+\sum_{i=1}^{6}\dfrac{\partial\mathbf{P}_{i}^{\text{S}}}{\partial y}\right)^{2}\\+\left(\dfrac{\partial\mathbf{P}^{\Omega}}{\partial z}+\sum_{i=1}^{6}\dfrac{\partial\mathbf{P}_{i}^{\text{S}}}{\partial z}\right)^{2}\end{array}\right\}\mathbf{C}_{m_1n_1l_1}^{2}rdrd\theta dz \tag{10}$$

where ρ_{pg} and ρ_{c} are the density of the plate and the cavity. The symbols ω_{pg} and ω_{c} are the circular frequencies of the plate and the cavity, respectively.

The total potential energy equations U of the coupling system are:

$$U_{\text{plate}}^{g}=\frac{1}{2}\int_{R_0}^{R_1}\int_{0}^{\phi}\left\{\begin{array}{l}D_{11}^{g}\left(\dfrac{\partial^{2}\mathbf{W}^{\Omega}}{\partial r^{2}}+\sum_{l=1}^{2}\dfrac{\partial^{2}\mathbf{W}_{l}^{\text{B}}}{\partial r^{2}}\right)^{2}\\+D_{22}^{g}\left[\left(\dfrac{\partial\mathbf{W}^{\Omega}}{r\partial r}+\sum_{l=1}^{2}\dfrac{\partial\mathbf{W}_{l}^{\text{B}}}{r\partial r}\right)+\left(\dfrac{\partial^{2}\mathbf{W}^{\Omega}}{r^{2}\partial\theta^{2}}+\sum_{l=1}^{2}\dfrac{\partial^{2}\mathbf{W}_{l}^{\text{B}}}{r^{2}\partial\theta^{2}}\right)\right]^{2}\\+2D_{12}^{g}\left(\dfrac{\partial^{2}\mathbf{W}^{\Omega}}{\partial r^{2}}+\sum_{l=1}^{2}\dfrac{\partial^{2}\mathbf{W}_{l}^{\text{B}}}{\partial r^{2}}\right)\left[\begin{array}{l}\left(\dfrac{\partial\mathbf{W}^{\Omega}}{r\partial r}+\sum_{l=1}^{2}\dfrac{\partial\mathbf{W}_{l}^{\text{B}}}{r\partial r}\right)\\+\left(\dfrac{\partial^{2}\mathbf{W}^{\Omega}}{r^{2}\partial\theta^{2}}+\sum_{l=1}^{2}\dfrac{\partial^{2}\mathbf{W}_{l}^{\text{B}}}{r^{2}\partial\theta^{2}}\right)\end{array}\right]\\+4D_{66}^{g}\left[\left(\dfrac{\partial^{2}\mathbf{W}^{\Omega}}{r\partial r\partial\theta}+\sum_{l=1}^{2}\dfrac{\partial^{2}\mathbf{W}_{l}^{\text{B}}}{r\partial r\partial\theta}\right)-\left(\dfrac{\partial^{2}\mathbf{W}^{\Omega}}{r^{2}\partial\theta^{2}}+\sum_{l=1}^{2}\dfrac{\partial^{2}\mathbf{W}_{l}^{\text{B}}}{r^{2}\partial\theta^{2}}\right)\right]^{2}\end{array}\right\}\left(\mathbf{A}_{mn}^{g}\right)^{2}rdrd\theta \tag{11}$$

$$D_{11}^{g}=\frac{E_{r}^{g}h_{\text{pg}}^{3}}{12\left(1-\mu_{r}^{g}\mu_{\theta}^{g}\right)},\quad D_{22}^{g}=\frac{E_{\theta}^{g}h_{\text{pg}}^{3}}{12\left(1-\mu_{r}^{g}\mu_{\theta}^{g}\right)}$$
$$D_{12}^{g}=\mu_{r}^{g}D_{22}^{g}=D_{21}^{g},\qquad D_{66}^{g}=G_{r\theta}^{g}h_{\text{pg}}^{3}/12 \tag{12}$$

$$U_{\text{cavity}}=\frac{1}{2\rho_{\text{c}}c_{0}^{2}}\int_{R_0}^{R_1}\int_{0}^{\phi}\int_{0}^{h_{\text{c}}}\left\{\left(\mathbf{P}^{\Omega}+\sum_{i=1}^{6}\mathbf{P}_{i}^{\text{S}}\right)^{2}\mathbf{C}_{m_1n_1l_1}^{2}\right\}rdrd\theta dz \tag{13}$$

in which E_{r}^{g} and E_{θ}^{g} are modulus, and G_{xy}^{g} is shear modulus. The relation of Poisson's ratios μ_{r}^{g} and μ_{θ}^{g} is: $\mu_{x}^{g}E_{y}^{g}=\mu_{y}^{g}E_{x}^{g}$. In addition, c_0 is sound velocity inside the cavity.

As mentioned earlier, the energy expression of the spring potential energy V_{spring}^{g} (g=1, 2) stored on the boundary of the orthotropic thin plate is expressed by artificial virtual spring technology. The realization of arbitrary boundary constrains is achieved by setting the spring stiffness of the four edges. The specific expressions of them can be obtained as:

$$V_{\text{spring}}^{g}=V_{\text{spring}}^{gr}+V_{\text{spring}}^{g\theta} \tag{14}$$

$$
\begin{aligned}
V_{\text{spring}}^{gr} &= \frac{1}{2}\int_0^{\phi} R_0 \left[k_{r0}\left(\mathbf{W}^{\Omega} + \sum_{l=1}^{4} \mathbf{W}_l^{\mathrm{B}} \right)^2 + K_{r0}\left(\frac{\partial \mathbf{W}^{\Omega}}{\partial r} + \sum_{l=1}^{4} \frac{\partial \mathbf{W}_l^{\mathrm{B}}}{\partial r} \right)^2 \right]_{r=R_0} \left(\mathbf{A}_{\text{plate}}^{g} \right)^2 d\theta \\
&+ \frac{1}{2}\int_0^{\phi} R_1 \left[k_{r1}\left(\mathbf{W}^{\Omega} + \sum_{l=1}^{4} \mathbf{W}_l^{\mathrm{B}} \right)^2 + K_{r1}\left(\frac{\partial \mathbf{W}^{\Omega}}{\partial r} + \sum_{l=1}^{4} \frac{\partial \mathbf{W}_l^{\mathrm{B}}}{\partial r} \right)^2 \right]_{r=R_1} \left(\mathbf{A}_{\text{plate}}^{g} \right)^2 d\theta
\end{aligned} \tag{15}
$$

$$
\begin{aligned}
V_{\text{spring}}^{g\theta} &= \frac{1}{2}\int_{R_0}^{R_1} \left[k_{\theta 0}\left(\mathbf{W}^{\Omega} + \sum_{l=1}^{4} \mathbf{W}_l^{\mathrm{B}} \right)^2 + K_{\theta 0}\left(\frac{\partial \mathbf{W}^{\Omega}}{r\partial \theta} + \sum_{l=1}^{4} \frac{\partial \mathbf{W}_l^{\mathrm{B}}}{r\partial \theta} \right)^2 \right]_{\theta=0} \left(\mathbf{A}_{\text{plate}}^{g} \right)^2 dr \\
&= \frac{1}{2}\int_{R_0}^{R_1} \left[k_{\theta 1}\left(\mathbf{W}^{\Omega} + \sum_{l=1}^{4} \mathbf{W}_l^{\mathrm{B}} \right)^2 + K_{\theta 1}\left(\frac{\partial \mathbf{W}^{\Omega}}{r\partial \theta} + \sum_{l=1}^{4} \frac{\partial \mathbf{W}_l^{\mathrm{B}}}{r\partial \theta} \right)^2 \right]_{\theta=\phi} \left(\mathbf{A}_{\text{plate}}^{g} \right)^2 dr
\end{aligned} \tag{16}
$$

The coupling potential energy is generated by mutual contact extrusion of sound pressure and vibration displacement between the contact surface of the orthotropic thin plate and the cavity, which can be expressed as:

$$
W_{\text{c-p}}^{g} = W_{\text{p-c}}^{g} = \int_{R_0}^{R_1}\int_0^{\phi} \left\{ \mathbf{A}_{mn}^{g} \mathbf{C}_{m_1 n_1 l_1} \left(\mathbf{W}^{\Omega} + \sum_{l=1}^{2} \mathbf{W}_l^{\mathrm{B}} \right) \left(\mathbf{P}^{\Omega} + \sum_{i=1}^{6} \mathbf{P}_i^{\mathrm{S}} \right) \right\} r dr d\theta \tag{17}
$$

W_{wall} expresses the dissipated acoustic energy of the impedance walls [9-11], which is:

$$
W_{\text{wall}} = -\frac{1}{2j\omega_{\text{c}}} \int_{S_q} \sum_{q=1}^{4} \left\{ \left(\mathbf{P}^{\Omega} + \sum_{i=1}^{6} \mathbf{P}_i^{\mathrm{S}} \right)^2 \Big/ Z_q \right\} \mathbf{C}_{m_1 n_1 l_1}^2 dS_q \tag{18}
$$

where j is the pure imaginary and expresses the circular frequency of the cavity. The corresponding impedance value for each wall surface S_q (q=1, 2, 3, 4) is Z_q which the complex acoustic impedance.

The work done by the point sound source W_{sound} can be written as:

$$
W_{\text{sound}} = -\frac{1}{j\omega_{\text{c}}} \int_{R_0}^{R_1}\int_0^{\phi}\int_0^{h_{\text{c}}} \left\{ Q\left(\mathbf{P}^{\Omega} + \sum_{i=1}^{6} \mathbf{P}_i^{\mathrm{S}} \right) \mathbf{C}_{m_1 n_1 l_1} \right\} r dr d\theta dz \tag{19}
$$

$$
Q = \frac{4\pi A}{j\rho_c c_0 k} \delta(r - r_0)\delta(\theta - \theta_0)\delta(z - z_0) \tag{20}
$$

in which A is the amplitude of the source (in kg/ s^2), δ is the 3D Dirac function. The wave number is $k=\omega_{\text{c}}/c_0$. The point sound source is located at (r0, θ_0 , z0).

2.4 Solution of Equation of the Structural-Acoustic Coupling System

The solving equation of the coupling system can be obtained on the basis of the Rayleigh-Ritz energy method, which can be expressed as:

$$
\frac{\partial L_{\text{plate}}^{g}}{\partial \mathbf{A}_{mn}^{g}} = \frac{\partial T_{\text{plate}}^{g}}{\partial \mathbf{A}_{mn}^{g}} - \frac{\partial U_{\text{plate}}^{g}}{\partial \mathbf{A}_{mn}^{g}} - \frac{\partial V_{\text{spring}}^{g}}{\partial \mathbf{A}_{mn}^{g}} - \frac{\partial W_{\text{c-p}}^{g}}{\partial \mathbf{A}_{mn}^{g}} = \mathbf{0} \tag{21}
$$

$$
\frac{\partial L_{\text{cavity}}}{\partial \mathbf{C}_{m_1 n_1 l_1}} = \frac{\partial T_{\text{cavity}}}{\partial \mathbf{C}_{m_1 n_1 l_1}} - \frac{\partial U_{\text{cavity}}}{\partial \mathbf{C}_{m_1 n_1 l_1}} - \frac{\partial W_{\text{wall}}}{\partial \mathbf{C}_{m_1 n_1 l_1}} + \sum_{g=1}^{2} \left(\frac{\partial W_{\text{p-c}}^{g}}{\partial \mathbf{C}_{m_1 n_1 l_1}} \right) - \frac{\partial W_{\text{sound}}}{\partial \mathbf{C}_{m_1 n_1 l_1}} = \mathbf{0} \tag{22}
$$

The more simplified solving equations can be rewritten as a matrix form :

$$
(\mathbf{K}_{\text{plate}}^{g} - \omega^2 \mathbf{M}_{\text{plate}}^{g}) \mathbf{A}_{mn}^{g} + \mathbf{C}_{\text{c-p}}^{g} \mathbf{C}_{m_1 n_1 l_1} = \mathbf{0} \tag{23}
$$

$$
(\mathbf{K}_{\text{cavity}} - \omega \mathbf{Z}_{\text{cavity}} - \omega^2 \mathbf{M}_{\text{cavity}}) \mathbf{C}_{m_1 n_1 l_1} + \omega^2 \sum_{g=1}^{2} \mathbf{C}_{\text{p-c}}^{g} \mathbf{A}_{mn}^{g} = \mathbf{Q} \tag{24}
$$

in which $\mathbf{K}_{\text{plate}}^{g}$ and $\mathbf{K}_{\text{cavity}}$ are stiffness matrices of the plate and the cavity. $\mathbf{M}_{\text{plate}}^{g}$ and $\mathbf{M}_{\text{cavity}}$ are the corresponding mass matrices . $\mathbf{Z}_{\text{cavity}}$ is the impedance matrix. Beside, $\mathbf{C}_{\text{c-p}}^{g}$ and $\mathbf{C}_{\text{p-c}}^{g}$ are the coupled matrices with the equality relation: $\mathbf{C}_{\text{p-c}}^{g}=\left(\mathbf{C}_{\text{c-p}}^{g}\right)^{T}$. $\mathbf{Q}$ is the sound source vector worked inside the cavity. But in Equation 24, circular frequency has linear terms and nonlinear terms. So, it needs to further transformation according to the Refs. [10, 12]:

$$\left(\overline{\mathbf{K}}-\omega\overline{\mathbf{M}}\right)\overline{\mathbf{G}}=\overline{\mathbf{F}} \tag{25}$$

Up to now, we can get the natural frequencies easily. At the same time, the displacement and sound pressure admissible function can also be gained.

3. NUMERICAL RESULTS AND DISCUSSIONS

In this part, a number of numerical simulations will be discussed to validate the applicability of the present method in analyzing the structure-acoustic system. In all the following numerical examples, the physical parameters of the air cavity and the water cavity are exactly the same, which include the mass density ρ_{air}=1.21kg/m^3, ρ_{water}=1000kg/m^3 and the speed of sound propagation c_{air}=340m/s and c_{water}=1480m/s. The various boundary conditions (BC) of the orthotropic plate are described by alphabetic strings. Specifically, F is free-edge, S is simply-support, C is clamped edge and E is elastic edge. The boundary conditions of the two plates are same.

3.1 Natural Characteristics Analysis of the Orthotropic Coupling System

Because the improved Fourier series method is used for the first time to analyse the orthotropic annular sector double-plate cavity coupling system, it is necessary to study its convergence and accuracy. Table 1 gives the convergence and accuracy analysis of the coupled natural frequency. The geometric parameters are defined as: R_1=1m, R_0=0.5m, h_{p1}=h_{p2}=0.005m, h_{c}=0.5m and ϕ=90$^{\text{o}}$. The material parameters of the two clamped plates are chosen as: E_1=20GPa, E_2=10GPa, G_{12}=5GPa, μ_{12}=0.25 and ρ_{p}=1600kg/m^3. As can be found from Table 2, take air as an example, the biggest difference for the worst case which is made the contrast of (8×8, 4×4×4) and (12×12, 6×6×6) is less than 0.13%. Therefore, the present method has shown good convergence. At the same time, the correctness of the present method has been verified through comparison with the results obtained by FEM.

Table 1. Convergence and accuracy analysis of the structure-acoustic system

Medium	Mp×Np	Mc×Nc×Qc	Mode number (Hz)							
			1	2	3	4	5	6	7	8
Air	8×8	4×4×4	74.784	80.632	82.872	84.570	102.979	103.749	128.852	130.803
		5×5×5	74.783	80.632	82.872	84.568	102.977	103.749	128.737	130.661
		6×6×6	74.783	80.632	82.871	84.568	102.976	103.747	128.737	130.661
	10×10	4×4×4	74.784	80.632	82.869	84.567	102.976	103.746	128.842	130.792
		5×5×5	74.783	80.632	82.868	84.565	102.974	103.746	128.726	130.650
		6×6×6	74.783	80.632	82.868	84.565	102.973	103.745	128.726	130.650
	12×12	4×4×4	74.784	80.632	82.868	84.567	102.976	103.745	128.839	130.788
		5×5×5	74.783	80.632	82.867	84.565	102.974	103.745	128.723	130.646
		6×6×6	74.783	80.632	82.867	84.565	102.972	103.744	128.723	130.646
	FEM		71.344	78.235	80.206	81.150	105.120	105.870	130.120	133.810
Water	8×8	4×4×4	12.968	15.524	19.402	23.224	26.410	35.837	38.653	50.995
		5×5×5	12.960	15.517	19.375	23.224	26.382	34.675	36.866	50.987

	6×6×6	12.960	15.516	19.375	23.196	26.351	34.668	36.866	49.065
10×10	4×4×4	12.965	15.524	19.400	23.222	26.409	35.820	38.639	50.986
	5×5×5	12.957	15.517	19.373	23.222	26.381	34.661	36.854	50.978
	6×6×6	12.957	15.516	19.373	23.194	26.349	34.653	36.854	49.057
12×12	4×4×4	12.964	15.524	19.400	23.222	26.409	35.818	38.636	50.983
	5×5×5	12.957	15.517	19.373	23.222	26.381	34.658	36.852	50.977
	6×6×6	12.956	15.516	19.372	23.194	26.349	34.650	36.852	49.050
FEM		12.488	13.636	18.601	23.494	26.911	37.190	39.729	46.453

For the study of this paper, the most important and fundamental objective is to understand the changes of the natural characteristics before and after the coupling. In Table 2, the frequencies of the upper plate, lower plate, acoustic cavity and coupled system have been given, respectively. The geometric parameters are defined as: R_1=1m, R_0=0.3m, h_{p1}=h_{p2}=0.005m, h_c=0.8m and ϕ=60^o. The material parameters of the upper clamped plate are chosen as: E_1=50GPa, E_2=10GPa, G_{12}=2GPa, μ_{12}=0.25 and ρ_p=1600kg/m^3, while the material parameters of the lower clamped plate are chosen as: E_1=20GPa, E_2=10GPa, G_{12}=5GPa, μ_{12}=0.25 and ρ_p=1600kg/m^3. From Table 2, it can be seen that the frequency of the coupled system with air as medium changes slightly after coupling, indicating that it is a weakly coupled system. Compared with the coupled system with air as medium, the natural frequencies of the coupled system with water as medium are small and dense. This is essentially the difference between strong and weak coupling effect caused by the physical characteristics of different acoustic medium.

Table 2. Coupling degree analysis of the coupled systems filled with air or water

Medium	Frequency type	Mode number (Hz)						
		1	2	3	4	5	6	7
	Upper plate	67.444	104.321	160.413	166.194	200.210	228.320	267.900
	Lower plate	53.350	95.540	118.585	152.496	169.202	215.320	220.892
Air	Acoustic cavity	212.500	226.198	254.643	310.357	331.661	405.904	417.828
	Coupled system	54.570	68.793	94.482	103.186	117.309	151.340	159.168
Water	Acoustic cavity	925.000	984.626	1108.445	1350.967	1443.702	1766.876	1818.783
	Coupled system	10.651	21.960	24.484	27.913	38.551	41.103	44.469

Next, Table 3 gives the natural frequencies of the coupled system under various elastic boundary conditions. The geometric parameters are defined as: R_1=1m, h_{p1}=h_{p2}=0.005m, h_c=0.8m and ϕ=60^o. The material parameters of the two plates are chosen as: E_1=20GPa, E_2=10GPa, G_{12}=5GPa, μ_{12}=0.25 and ρ_p=1600kg/m^3. It can be found from Table 3 that the radius ratio and boundary condition have an important effect on the natural characteristics of the coupled system. Specifically, the natural frequency will increase with the increase of radius ratio and spring stiffness.

Table 3. Natural frequencies of the coupled system under various elastic boundary conditions

Medium	R_0/R_1	BC	Mode number (Hz)							
			1	2	3	4	5	6	7	8
Air	0.2	EFEF	24.729	29.149	29.183	37.463	53.488	53.494	60.492	60.781
		EEEE	43.876	51.237	74.088	74.232	79.784	79.947	105.423	106.200
		ECEC	47.630	53.728	86.008	86.114	93.173	93.349	130.086	130.845
	0.6	EFEF	70.370	71.777	72.110	77.536	77.559	78.684	94.258	94.263
		EEEE	73.972	79.990	87.505	87.860	111.005	112.541	133.148	133.184
		ECEC	85.959	90.546	104.904	105.253	138.246	139.266	184.102	185.136
Water	0.2	EFEF	3.852	5.996	6.270	10.972	11.881	14.097	14.143	15.868
		EEEE	7.224	14.615	15.338	15.493	16.290	24.206	25.314	27.662

	ECEC	8.234	18.778	19.462	19.623	20.513	32.815	34.707	37.809
0.6	EFEF	10.361	12.212	13.427	18.880	18.976	27.360	27.364	31.659
	EEEE	11.519	15.838	17.326	25.749	26.331	33.309	33.430	38.038
	ECEC	14.483	21.087	22.721	35.421	36.355	51.195	51.892	55.956

3.2 Forced Response Analysis of The Orthotropic Coupling System

The next section focuses on the difference of the forced response between the weak and strong coupling system. The geometric parameters and the material parameters used in Figure 2 are exactly the same as those used in Table 1. The unit point sound source is applied at ($R/4$, $\phi/4$, $h_c/4$). It can be seen from Figure 2 that the response curves between the weak coupling system filled with air and the strong coupling system filled with water are very different. An obvious difference is that the response amplitude of the strong coupling system is lower compared with the weak coupling system, which indicates that the consumption of water to external excitation is more significant.

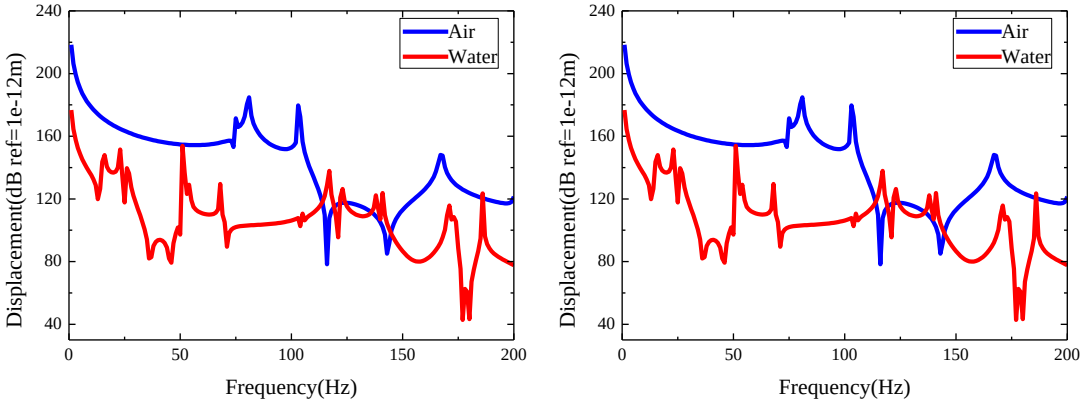

(a) displacement at ($R/2$, $\phi/2$) (b) sound pressure at ($R/2$, $\phi/2$, $h_c/2$)

Figure 2:Response of the coupled system with different acoustic medium

Next, Figure 3 shows the response curves of the coupled system filled with air under different impedance boundary conditions. The impedance boundary conditions of the air cavity are set to be: rigid and $Z=\rho_c c_0(50\text{-}j)$ on the four uncoupled walls. The unit point sound source is applied at ($R/8$, $\phi/8$, $h_c/8$). From Figure 3 we can find that the peak values of the response curves decrease with the increase of the number of the impedance walls. And no matter what impedance boundary conditions, the trend of the curves is not affected.

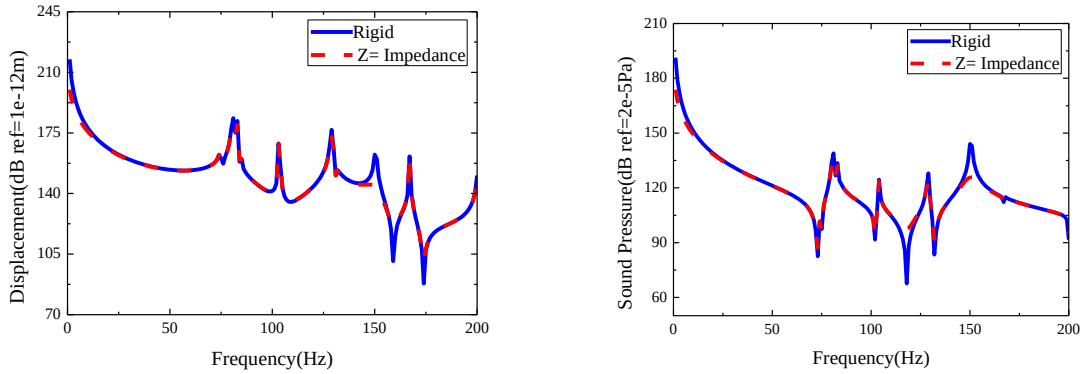

(a) displacement at ($3R/8$, $3\phi/8$) (b) sound pressure at ($3R/8$, $3\phi/8$, $h_c/4$)

Fig.3 Response of the coupled system filled with air under different impedance boundary conditions

4. CONCLUSIONS

In this paper, an orthotropic annular sector double-plate cavity coupling system is established to study the vibro-acoustic coupling characteristics. Based on the study on the natural characteristics of the coupled systems, the sound pressure and displacement responses under the excitation of a point sound source with various impedance boundary conditions have been studied. The results obtained by the present method have been compared with those obtained by FEM. On this basis, some new results and conclusions are given:

(1) The coupling system filled with air is weakly coupled system and the coupling system filled with water is strongly coupled system.

(2) The natural frequency will increase with the increase of radius ratio and spring stiffness.

(3) The response amplitude of the strong coupling system is lower compared with the weak coupling system, which indicates that the consumption of water to external excitation is more significant.

(4) The peak values of the response curves decrease with the increase of the number of the impedance walls. And no matter what impedance boundary conditions, the trend of the curves is not affected.

5. ACKNOWLEDGEMENTS

This paper is funded by the International Exchange Program of Harbin Engineering University for Innovation-oriented Talents Cultivation. The works also supported by the National Natural Science Foundation of China (No. 51679056), and Natural Science Foundation of Heilongjiang Province of China (E2016024).

6. REFERENCES

1. Li, D., L. Cheng, and C. Gosselin, Analysis of structural acoustic coupling of a cylindrical shell with an internal floor partition. Journal of Sound and vibration, 2002. 250(5): p. 903-921.

2. Henry, J.K. and R. Clark, Active control of sound transmission through a curved panel into a cylindrical enclosure. Journal of Sound and Vibration, 2002. 249(2): p. 325-349.

3. Henry, J.K. and R.L. Clark, Noise transmission from a curved panel into a cylindrical enclosure: Analysis of structural acoustic coupling. The Journal of the Acoustical Society of America, 2001. 109(4): p. 1456-1463.

4. Gardonio, P., N. Ferguson, and F. Fahy, A modal expansion analysis of noise transmission through circular cylindrical shell structures with blocking masses. Journal of Sound and Vibration, 2001. 244(2): p. 259-297.

5. Lee, Y., Insertion loss of a cavity-backed semi-cylindrical enclosure panel. Journal of sound and vibration, 2003. 259(3): p. 625-636.

6. Yao, S., et al., Sound reduction by metamaterial-based acoustic enclosure. AIP Advances, 2014. 4(12): p. 124306.

7. da Rocha, J., A. Suleman, and F. Lau, Flow-induced noise and vibration in aircraft cylindrical cabins: closed-form analytical model validation. Journal of Vibration and Acoustics, 2011. 133(5): p. 051013.

8. Pan, X., et al. Investigation of sound radiation from a water-loaded cylindrical enclosure due to airborne noise. in Proc Acoustics. 2013.